To appear in Spacebound-97, Canadian Space Agency

FINITE ELEMENT ANALYSIS OF MAGNETIC DAMPING EFFECTS ON G-JITTER INDUCED FLUID FLOW

Bo Pan and B. Q. Li
Department of Mechanical Engineering
Louisiana State University
Baton Rouge, LA 70803

and

H. C. de Groh
NASA Lewis Research Center
Cleveland, OH 44135

ABSTRACT

This paper reports some interim results on numerical modeling and analyses of magnetic damping of g-jitter driven fluid flow in microgravity. A finite element model is developed to represent the fluid flow, thermal and solute transport phenomena in a 2-D cavity under g-jitter conditions with and without an applied magnetic field. The numerical model is checked by comparing with analytical solutions obtained for a simple parallel plate channel flow driven by g-jitter in a transverse magnetic field. The model is then applied to study the effect of steady state g-jitter induced oscillation and on the solute redistribution in the liquid that bears direct relevance to the Bridgman-Stockbarger single crystal growth processes. A selection of computed results is presented and the results indicate that an applied magnetic field can effectively damp the velocity caused by g-jitter and help to reduce the time variation of solute redistribution.

1. INTRODUCTION

It is well known that natural convection affects the diffusional growth of crystals from melts. Microgravity environment in space vehicles has provided a unique means by which the unwanted convective flows induced by gravity can be significantly reduced. However, the space environment often reveals effects that are not known or present on Earth. One of these effects is g-jitter or residual acceleration phenomena associated with microgravity environment. Residual accelerations or g-jitter occurring during space processing of melts, such as the melts from which single crystals are grown, can cause appreciable convective flows, making it difficult to realize diffusion controlled single crystal growth in space[1].

G-jitter comes from crew motions, mechanical vibrations (pumps, motors, excitations of natural frequencies of spacecraft structures), spacecraft maneuvers and attitude, atmosphere drag and the Earth's gravity gradient [2]. Studies on g-jitter effects indicate that convection in

microgravity is related to the magnitude and frequency of g-jitter and to the alignment of the gravity field with respect to the growth direction or the direction of the temperature gradient [3-6]. A residual gravity of 10^{-5} g_o, where g_o is the Earth gravity constant, is sufficient to cause unacceptable fluid motion in the liquid, unacceptable in the sense that the g-jitter induced flow is intensive enough to affect deleteriously the solute distribution in the melt and hence the quality of the crystal grown. The orientation of the gravity vector with respect to the temperature gradient plays also an important role in melt flows. The velocity attains a maximum when the gravity vector is perpendicular to the temperature gradient.

Numerous attempts have been made to estimate and calculate the adverse effects of time varying g-jitter [6-11]. These calculations are all based on numerical models. Both 2D and 3D numerical models have been developed for this purpose [4,12]. These models have been used to study the effects associated with both idealized single- and multiple-frequency g-jitter modulations and realistic g-jitter data collected by accelerometer during actual flight experiments. These studies showed that the frequency, amplitude and spatial orientation of the residual gravity vector all play an important role in determining the convective flow behavior of the system. When the residual accelerations oscillate about the positive and negative of an axis, the orientation of this direction relative to the density gradient determines whether a mean flow is generated in the system [11]. Sinusoidal oscillating accelerations induce an oscillating convective flow and composition oscillation in the liquid. The resultant velocity and composition fields oscillate with the same frequency of the affecting gravity field.

These studies have shed light on the basic nature of g-jitter effects and have provided a thrust to devise useful mechanisms to suppress g-jitter induced convective flows. One technique is to apply the principle of magnetic damping to achieve the velocity reduction. Magnetic damping is less effective than reducing gravity for convection reduction. It originates from the interaction of the flow field of an electrically conducting fluid and an applied magnetic field. This interaction gives rise to an opposing Lorentz force that reduces or damps the flow velocities in the liquid. Application of a magnetic field has been found to be effective in controlling convection during crystal growth from melts under terrestrial conditions and has now been widely practiced in the metals and semiconductor industries [13]. While there has been a large amount of literature addressing both the basic characteristics of g-jitter induced flows and application of magnetic damping to convection control in melt growth on Earth, little research work has been done on the assessment of the magnetic field effect on the convective flow associated with g-jitter in microgravity.

In this paper, a numerical analysis is presented of g-jitter driven flows and their effects on the solutal element distributions in a simplified Bridgman-Stockbarger crystal growth system. The numerical model is based on the solution of the Navier-Stokes equations for fluid flow, the energy balance equation for the temperature distribution and the mass balance equation for the species transport in a Ga-doped germanium melt. The model is applied to study the magnetic damping effects on the oscillating convective flows driven by g-jitter and on the solutal redistribution in the melts. Both single and multi-frequency g-jitter effects are studied and numerically obtained solutions are compared with available analytical solutions whenever possible.

2. PROBLEM STATEMENT

Figure 1 shows a simplified 2-D version of the Bridgman-Stockbarger single crystal growth process under microgravity condition, along with the coordinate system for analyses. The crystal-melt interface is located at z=0 and the melt is fed into the melt pool of height L from above. The width of the cavity is W, which is set equal to the height. The temperature at the crystal-melt interface is kept at T_m, and that at the inlet and the upper side walls is held at a higher temperature T_h. The lower side walls are adiabatic zones. The origin of the coordinate system is at the lower left corner of the cavity. In this system solidification of a dilute two-component melt takes place as the ampoule is translated through fixed hot and cold zones. Translation of the ampoule is simulated by supplying a doped melt bulk composition c_m and the density ρ_m at a constant velocity V_m at the top of the computational space (inlet). The ampoule is fed into the melt zone and the solidified alloy of composition $c_s=c_s(x,t)$ is withdrawn from below [4].

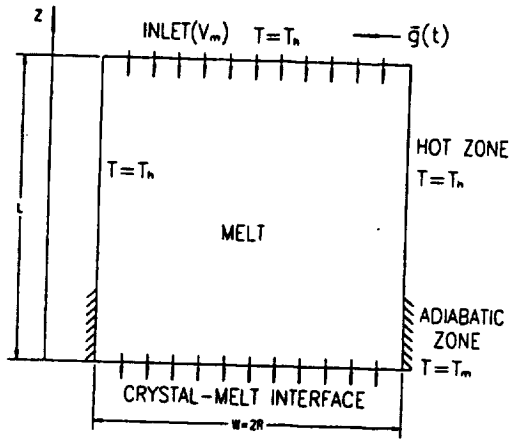

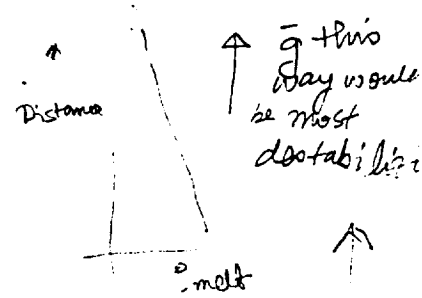

Figure 1. Schematic representation of the natural convection problems in a 2-D cavity in microgravity environment.

In a typical microgravity environment, the residual acceleration experienced by the spacecraft is composed of a steady component and a time-dependent component. The magnitude of the time-dependent component is much greater than that of the steady component. In this paper we consider the time dependent acceleration (g-jitter) represented by the following expression:

$$\mathbf{g}(t) = \sum_{n=1}^{N} g_n \sin(2\pi f_n t)\,\mathbf{e} \qquad (1)$$

where g_n and f_n are the amplitude and frequency of g-jitter respectively. The direction of the residual gravity is parallel to the crystal-melt interface, which has the most detrimental effects in terms of convective flows [4]. The above crystal growth system is immersed in a transverse magnetic field, which is intended to damp the convection resulting from g-jitter.

Our primary objective is to study the g-jitter-driven melt flow and the effect of the magnetic field on the flow in the crystal growth system as described above. To simplify the analysis, the solidification phenomena are not considered and the melt-crystal interface is held flat. The melt

flow, heat and mass transport in the 2-D cavity as illustrated in Figure 1 are governed by the continuity equation, the Navier-Stokes equations, the energy balance equation and the species conservation equation. These equations may be written in a nondimensionalized form as follows,

Equation of Continuity:

$$\nabla \bullet \mathbf{u} = 0 \tag{2}$$

Equation of Momentum Balance:

$$\frac{\partial \mathbf{u}}{\partial t} + \mathbf{u} \bullet \nabla \mathbf{u} = -\nabla p + \mathrm{Pr}\nabla^2 \mathbf{u} - Ra\mathrm{Prg}^* T + Ha^2 \mathrm{Pr}(\mathbf{u} \times \mathbf{b} \times \mathbf{b}) \tag{3}$$

Equation of Energy Balance:

$$\frac{\partial T}{\partial t} + \mathbf{u} \bullet \nabla T = \nabla^2 T \tag{4}$$

Equation of Solute Transport:

$$\frac{Sc}{\mathrm{Pr}}\left(\frac{\partial C}{\partial t} + \mathbf{u} \bullet \nabla C\right) = \nabla^2 C \tag{5}$$

where $\mathbf{u}=(u_x,u_y)$ is velocity field, p the pressure, **b** applied magnetic field, T the temperature, C the concentration of solutal element. The last term in Equation (3) represents the effect of the Lorentz force that arises from the application of an external magnetic field. In the above equations, the velocity is scaled by κ/L, the time by L^2/κ, the pressure by $\rho\kappa^2/L^2$. The temperature is defined by $(T(\mathbf{r},t)-T_m)/(T_h-T_m)$ where $T(\mathbf{r},t)$ is the dimensional temperature. The dimensionless parameters, that is, *Ra* the Rayleigh number, *Ha* the Hartmann number, *Pr* the Prandtl number, *Pe* the Peclet number and *Sc* the Schmidt number, are defined as:

$$Ra = \frac{\beta g(T_n - T_m)L^3}{\nu\kappa},\quad Ha = B_0 L\sqrt{\frac{\sigma}{\mu}},\quad \mathrm{Pr} = \frac{\nu}{\kappa},\quad Pe_g = \frac{VgL}{D},\quad Sc = \frac{\nu}{D}.$$

The boundary conditions for the system under consideration are given by:

$$T = 1,\quad \mathbf{u} \bullet \mathbf{n} = \frac{Pe_g \mathrm{Pr}}{Sc},\quad \mathbf{u} \times \mathbf{n} = 0,\quad \frac{\partial C}{\partial z} = Pe_g(1-k)C;\quad \text{at } z=0$$

$$T = 0,\quad \mathbf{u} \bullet \mathbf{n} = \frac{Pe_g \mathrm{Pr}}{Sc},\quad \mathbf{u} \times \mathbf{n} = 0,\quad \frac{\partial C}{\partial z} = Pe_g(C-1);\quad \text{at } z=1$$

$$\mathbf{u}\bullet\mathbf{n}=\frac{Pe_g\,\mathrm{Pr}}{Sc},\qquad \mathbf{u}\bullet\mathbf{e}_w=0,\qquad \mathbf{e}_w\bullet\nabla C=0;\ \text{along the two sides}$$

$T=1$ along the hot zone side; and $\mathbf{e}_w\bullet\nabla T=0$ along the adiabatic zone

where $\mathbf{n}$ is the unit vector normal to the planar crystal-melt interface, $\mathbf{e}_w$ the normal to the side wall, and k is the solute segregation coefficient.

3. FINITE ELEMENT SOLUTION

The above governing equations along with the boundary conditions are solved using the Galerkin finite element method. The stiffness matrix is obtained by using Galerkin's method of Weighted Residuals. Within each element, the dependent variables **u**, P, T, C are interpolated by shape functions of ϕ, ψ, and θ. Then the velocity, pressure, temperature and concentration fields are approximated by:

$$u_i(x,t)=\phi^T\mathbf{U}_i(t) \tag{6}$$

$$P(x,t)=\psi^T\mathbf{P}(t) \tag{7}$$

$$T(x,t)=\theta^T\mathbf{T}(t) \tag{8}$$

$$C(x,t)=\theta^T\mathbf{C}(t) \tag{9}$$

where $\mathbf{U}_i$, **P**, **T** and **C** are column vectors of element nodal point unknowns.

Substituting the above equations into the governing equations, we get the residuals of R_1, R_2, R_3 and R_4 which represent the momentum, mass conservation, energy and species equations respectively. The Galerkin form of the Method of Weighted Residuals seeks to reduce these errors to zero, and the shape functions are chosen the same as the weighting functions. Following the procedures given in [17], the governing equations may be written as:

Momentum

$$\begin{aligned}&\left(\int_v\phi\phi^T dV\right)\frac{\partial\mathbf{U}_i}{\partial t}+\left(\int_v\phi\,\mathbf{u}\bullet\nabla\phi^T dV\right)\mathbf{U}_i-\left(\int_v\psi\nabla\phi^T dV\right)\mathbf{P}\\&+\left(\int_v\mathrm{Pr}\nabla\phi\bullet\nabla\phi^T dV\right)\mathbf{U}_i+\left(\int_v\mathrm{Pr}\nabla\phi\nabla\phi^T dV\right)\bullet\mathbf{U}_i{}^T+\left(\int_v Ra\mathrm{Pr}\phi\theta^T\mathbf{g}\right)\mathbf{T}\\&=\int_s\tau\phi\,dS+\int_v Ha^2\mathrm{Pr}(\mathbf{u}\times\mathbf{b}\times\mathbf{b})dV\end{aligned} \tag{10}$$

Continuity (penalty formulation)

$$\left(\int_v\psi\nabla\phi^T dV\right)\mathbf{U}_i=-\varepsilon\left(\int_v\psi\psi^T dV\right)\mathbf{P} \tag{11}$$

Energy

$$\left(\int_v\theta\theta^T dV\right)\frac{d\mathbf{T}}{dt}+\left(\int_v\theta\,\mathbf{u}\bullet\nabla\theta^T dV\right)\mathbf{T}+\left(\int_v\nabla\theta\bullet\nabla\theta^T dV\right)\mathbf{T}=-\int_v q_T\theta\,ds \tag{12}$$

Species

$$\left(\int_v \frac{Sc}{\mathrm{Pr}}\theta\theta^T dV\right)\frac{d\mathbf{C}}{dt}+\left(\int_v \frac{Sc}{\mathrm{Pr}}\theta\mathbf{u}\bullet\nabla\theta^T dV\right)\mathbf{C}+\left(\int_v \nabla\theta\bullet\nabla\theta^T dV\right)\mathbf{C}=-\int_v q_c\theta\, ds \qquad (13)$$

Once the form of shape functions ϕ, θ, and ψ are specified, the integrals defined in above equations can be expressed by the matrix equation. Combining the momentum and energy equations into a single matrix equation, we get the element stiffness matrix equation:

$$\begin{bmatrix}\mathbf{M} & 0 & 0\\ 0 & \mathbf{N}_T & 0\\ 0 & 0 & \mathbf{N}_C\end{bmatrix}\begin{bmatrix}\dot{\mathbf{U}}\\ \dot{\mathbf{T}}\\ \dot{\mathbf{C}}\end{bmatrix}+\begin{bmatrix}\mathbf{A}(\mathbf{U})+\mathbf{K}+\frac{1}{\varepsilon}\mathbf{E}\mathbf{M}_p^{-1}\mathbf{E}^T & \mathbf{B} & 0\\ 0 & \mathbf{D}_T(\mathbf{U})+\mathbf{L}_T & 0\\ 0 & 0 & \mathbf{D}_C(\mathbf{U})+\mathbf{L}_C\end{bmatrix}\begin{bmatrix}\mathbf{U}\\ \mathbf{T}\\ \mathbf{C}\end{bmatrix}=\begin{bmatrix}\mathbf{F}\\ \mathbf{G}_T\\ \mathbf{G}_C\end{bmatrix} \qquad (14)$$

Note that in constructing the above element matrix equation, the penalty formulation has been applied, and $\mathbf{P}$ in the momentum equation is substituted by $\frac{1}{\varepsilon}\mathbf{M}_p^{-1}\mathbf{E}^T\mathbf{U}$. The assembled global matrix equations are stored in the skyline form and solved using the Gaussian elimination method. The coefficient matrices of above are defined by:

$$\mathbf{M}=\int_v \phi\phi^T dV$$

$$\mathbf{M}_p=\int_v \psi\psi^T dV$$

$$\mathbf{N}_T=\int_v \theta\theta^T dV \qquad \mathbf{N}_C=\int_v \frac{Sc}{\mathrm{Pr}}\theta\theta^T dV$$

$$\mathbf{K}=\int_v \mathrm{Pr}\nabla\phi\nabla\phi^T dV$$

$$\mathbf{E}=\int_v (\nabla\phi)\psi^T dV$$

$$\mathbf{L}_T=\int_v \nabla\theta\bullet\nabla\theta^T dV \qquad \mathbf{L}_C=\int_v \nabla\theta\bullet\nabla\theta^T dV$$

$$\mathbf{A}(\mathbf{U})=\int_v \phi\mathbf{u}\bullet\nabla\phi^T dV$$

$$\mathbf{D}_T(\mathbf{U})=\int_v \theta\mathbf{u}\bullet\nabla\theta^T dV \qquad \mathbf{D}_C(\mathbf{U})=\int_v \frac{Sc}{\mathrm{Pr}}\theta\mathbf{u}\bullet\nabla\theta^T dV$$

$$\mathbf{B}=\int_v Ra\mathrm{Pr}g\phi\theta^T dV$$

$$\mathbf{F}=\int_s \tau\phi\, dS+\int_v Ha^2\mathrm{Pr}(\mathbf{u}\times\mathbf{b}\times\mathbf{b})dV$$

$$\mathbf{G}_T=-\int_s q_T\theta\, dS \qquad \mathbf{G}_C=-\int_s q_C\theta\, dS$$

4. RESULTS AND DISCUSSION

The finite element model described above enables the prediction of the transient convective flows driven by g-jitter, the temperature distribution and the solutal redistribution in the melt

with and/or without an applied magnetic field. The calculations were performed using a finite element code that was developed by our research group. The code employs the backward Euler (or implicit) time scheme, with automatic time step control, and the penalty method for pressure approximation. The computer code was checked against other available commercial flow codes, including FIDAP, and analytical solutions for a wide variety of flows and thermal problems. A selection of results are presented below and the parameters used for calculations are given in Table 1. The transient calculations are started with an initial thermal and fluid flow field obtained with a constant gravity field; for the results in Figures 3-10 the initial flow field is generated with $g=10^{-6}g_0$, and those in Figures 11 and 12 are started with $g=10^{-5}g_0$, both parallel to the crystal-melt interface.

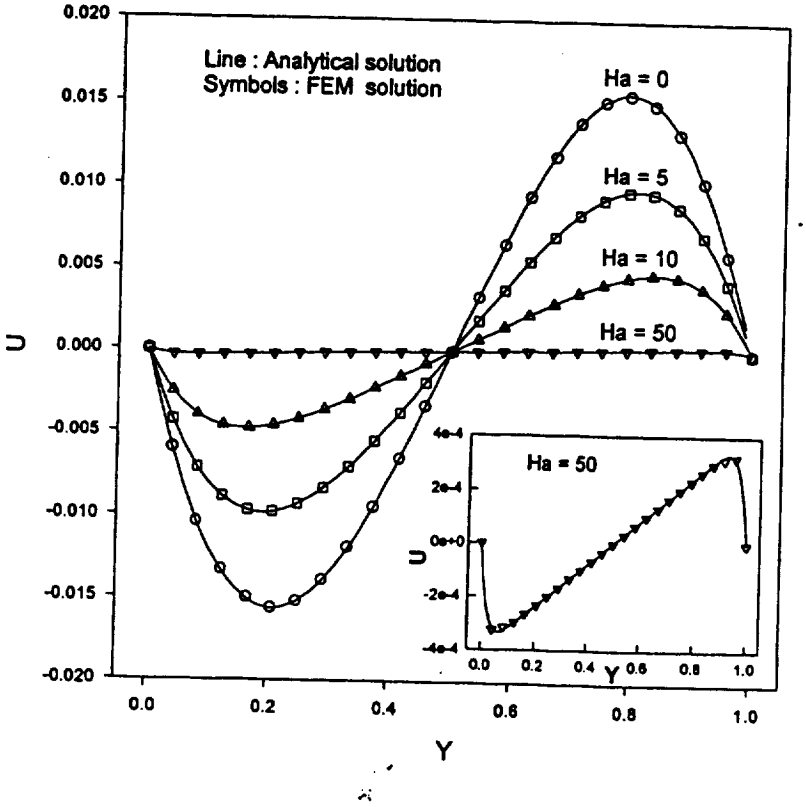

Figure 2. Comparison of the numerical and the analytical solutions for convective flows in a parallel plate channel: Y the location between the plate and U the fluid flow velocity, both nondimensionalized.

To further assess the code predictability for the magnetic damping effects on g-jitter driven flows, the finite element results are compared with the analytical solutions obtained for convective flows in a simple parallel plate geometry subject to a transverse magnetic field [18]. The height-to-width aspect ratio is set at 5, which was found to be sufficient to simulate the infinitely long geometry. The results are shown in Figure 2. Clearly the numerical results compare very well with the analytical solutions.

Table 1: Parameters used in calculations [4]

Property	Value
Thermal conductivity of the melt (k)	17 $WK^{-1}m^{-1}$
Heat capacity of the melt (C_p)	0.39 $J\,g^{-1}K^{-1}$
Density of the melt (ρ_M)	5.6×10^{3} $Kg\,m^{-3}$
Kinematic viscosity of the melt (ν)	1.3×10^{-7} m^2s^{-1}
Solute diffusivity (D)	1.3×10^{-8} m^2s^{-1}
Thermal diffusivity of the melt (κ)	1.3×10^{-5} m^2s^{-1}
Thermal expansion coefficient (β)	2.5×10^{-4} K^{-1}
Associated dimensionless parameters	**Value**
Prandtl number (Pr)	0.01
Peclet number (Pe)	5.0
Rayleigh number (Ra)	1.45×10^{3} (on earth value)
Hartmann number (Ha)	10 ~ 100
Schmidt number (Sc)	10

Operating conditions	Value
Hot zone temperature (T_h)	1331 K
Distance between inlet and interface (L)	0.01 m
Interface temperature (T_m)	1231 K
Translation rate (V_m)	6.5×10^{-6} $m\,s^{-1}$
Gravity (g)/ Frequency (Hz):	10^{-2}, 10^{-3}, $10^{-4}g_0$/1, 0.1, 0.01
Magnetic field B_0	0.022~0.22 T

* $1g_0 = 9.8\ m\,s^{-2}$

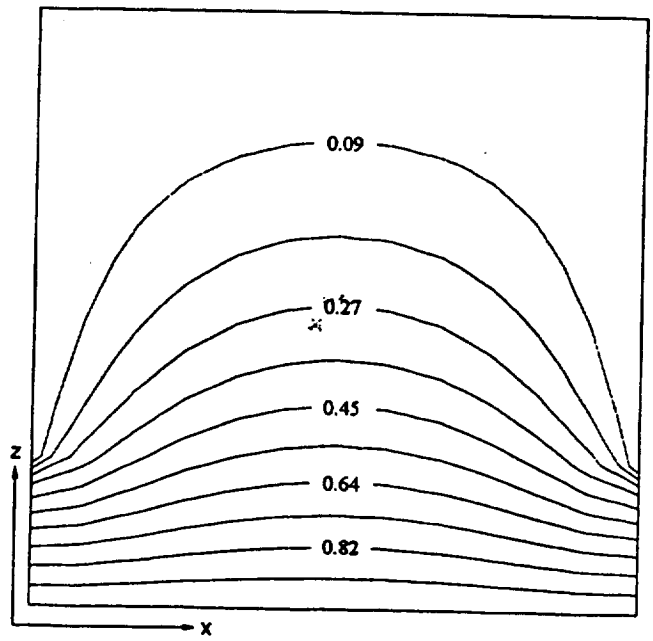

Figure 3. Temperature distribution in the 2-D cavity; thermal transport in the system is primarily attributed to conduction.

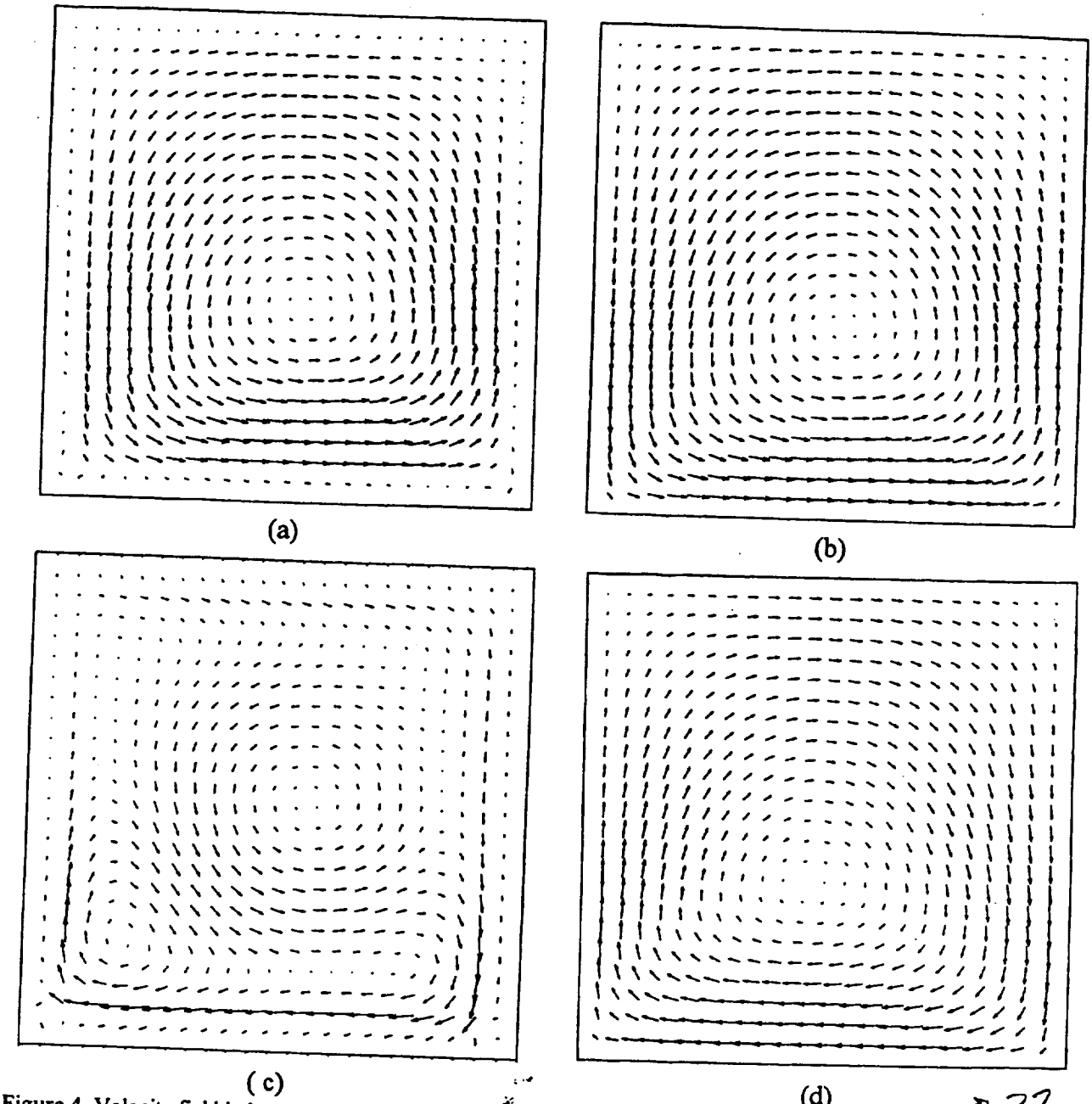

Figure 4. Velocity field induced by multi-frequency g-jitter, without the absence of a magnetic filed. (a) t = 0.5, Vmax = 0.139; (b) t = 1.75, Vmax = 0.24;(c) t = 2.5, Vmax = 0.06; (d) t = 10.25, Vmax = 0.218. (V and t are nondimensionalized.)

With the numerical model, the g-jitter driven flows, thermal field and solutal redistribution in the system can be analyzed. Figure 3 depicts the temperature distribution predicted in the system. For all the cases studied, the temperature profile remains basically the same and is practically unaffected by the natural convection in the pool. This is as expected because the Prandtl number is small for the melt being studied ($Pr=\nu/\kappa=0.01$) and thermal transport is dominated by conduction.

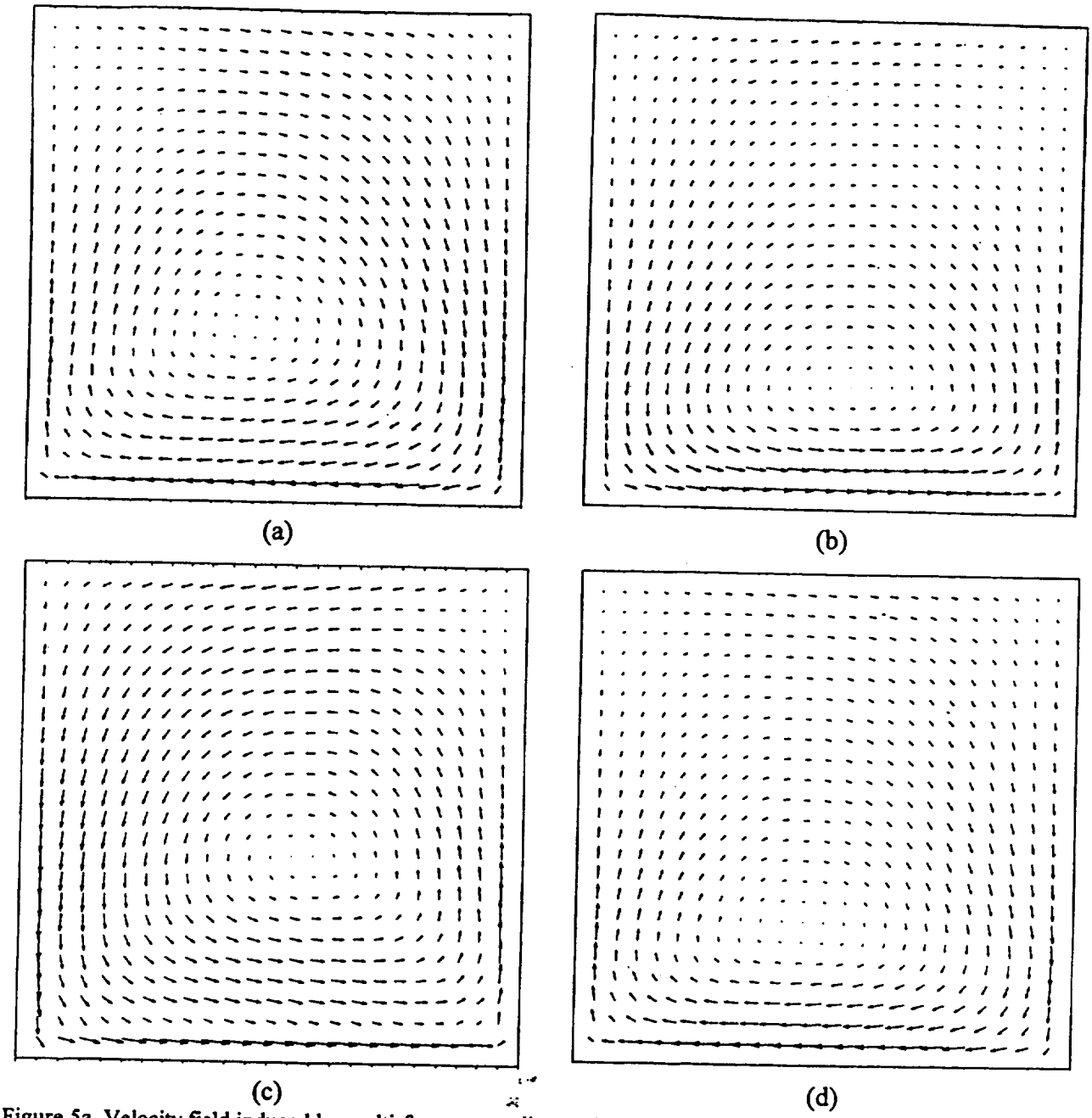

Figure 5a. Velocity field induced by multi-frequency g-jitter, with the presence of a magnetic filed, Bx = 0.22(B in x direction), Ha = 100. (a) t = 0.5, Vmax = 0.082; (b) t = 1.75, Vmax = 0.112; (c) t = 2.5, Vmax = 0.050;(d) t = 10.25, Vmax = 0.122. (V and t are nondimensionalized.)

Figures 4 and 5 show the basic fluid flow structure development in the melt pool with and without an applied magnetic field. The magnetic field effect on the g-jitter induced flows is further illustrated in Figure 6, where the maximum velocity (U component) in the pool is plotted as a function of time for the cases with and without an applied magnetic field. For the case considered, an application of a somewhat moderate magnetic field results in a reduction of velocity level by almost 50%. The magnetic damping effects are also related to the applied magnetic field strengths and the field directions, as shown in Figure 7. The higher the applied

magnetic field strength, the more the damping effect is. Also, the results plotted in Figure 7 suggest that for the case studied, the magnetic field, when oriented parallel to the thermal gradient, is more effective in reducing the velocity level in the liquid pool.

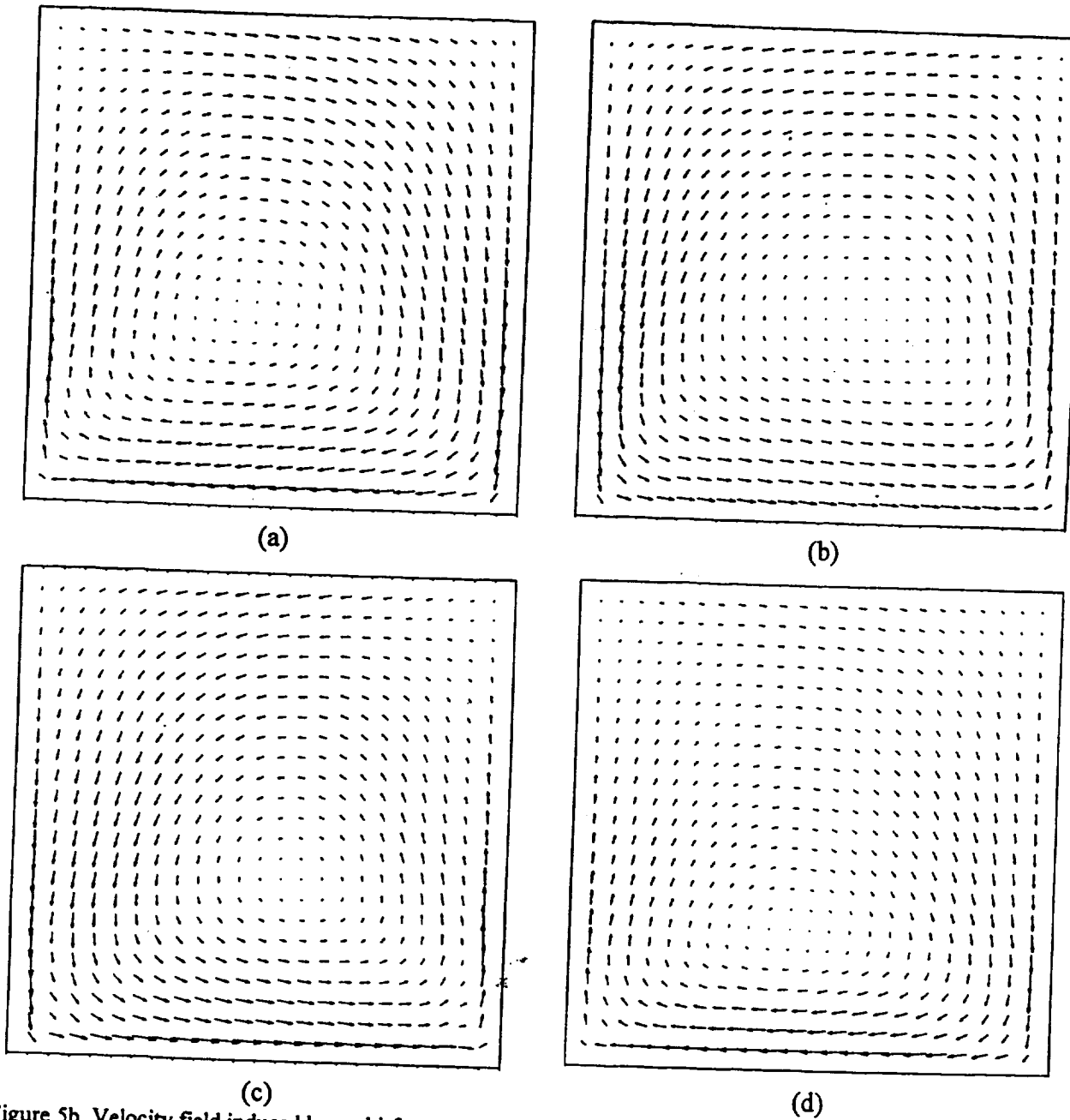

Figure 5b. Velocity field induced by multi-frequency g-jitter, with the presence of a magnetic filed, By = 0.22 (B in y direction) , Ha = 100. (a) t = 0.5, Vmax = 0.072; (b) t = 1.75, Vmax = 0.079; (c) t = 2.5, Vmax = 0.053;(d) t = 10.25, Vmax = 0.094. (V and t are nondimensionalized.)

The convection in the liquid pool can have a significant effect on the solutal distribution during crystal growth. To investigate this effect, the time dependent concentration profiles in liquid pool are plotted in Figures 8 and 9. From Figure 8, it is seen that the concentration

evolves as time continues and the g-jitter induced flow strongly affects the solutal transport in the melt. With an applied magnetic field, the liquid convection is reduced and hence its effect on the solutal distribution is also reduced, as appears in Figure 10. Figure 10 compares the time variation of the concentrations at two points in the melt pool. Apparently, with an applied magnetic field, the concentration oscillation is also greatly reduced .

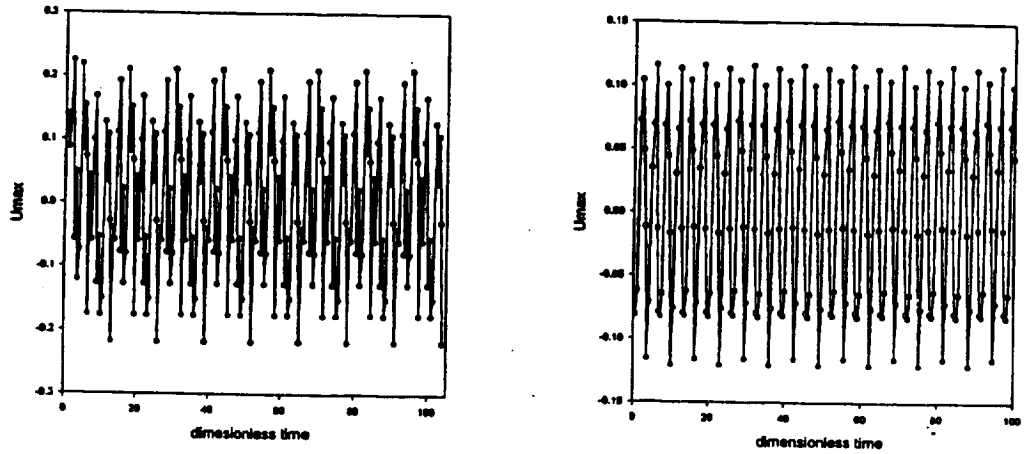

(a) (b)

Figure 6. Variation of maximum flow velocity in the Ga-doped germanium melt as affected by g-jitter and an applied magnetic field: (a) $g=10^{-2}$, 10^{-3}, 10^{-4}, fn=1,0.1,0.01, B=0; and (b) $g=10^{-2}$, 10^{-3}, 10^{-4}, fn=1,0.1,0.01, Bx=0.22 Tesla, Ha=100. Gravity oscillates parallel to the crystal-melt interface.

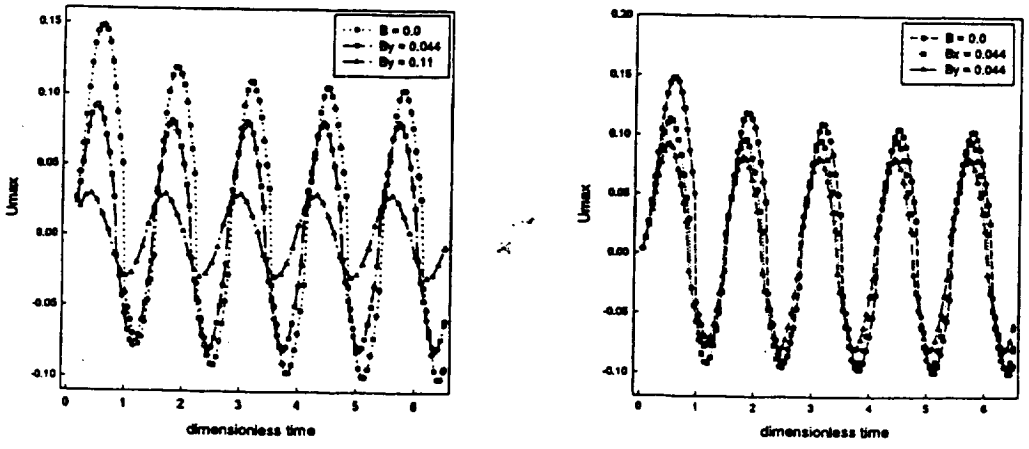

(a) (b)

Figure 7. Dependency of transient maximum flow velocity in the Ga-doped germanium melt on the direction and magnitude of the applied magnetic field: (a) effect of applied field strengths and (b) the effect of magnetic field directions. Other conditions: single frequency g-jitter, $g=10^{-3}$ and $f_n=0.1$ acting in the x-direction.

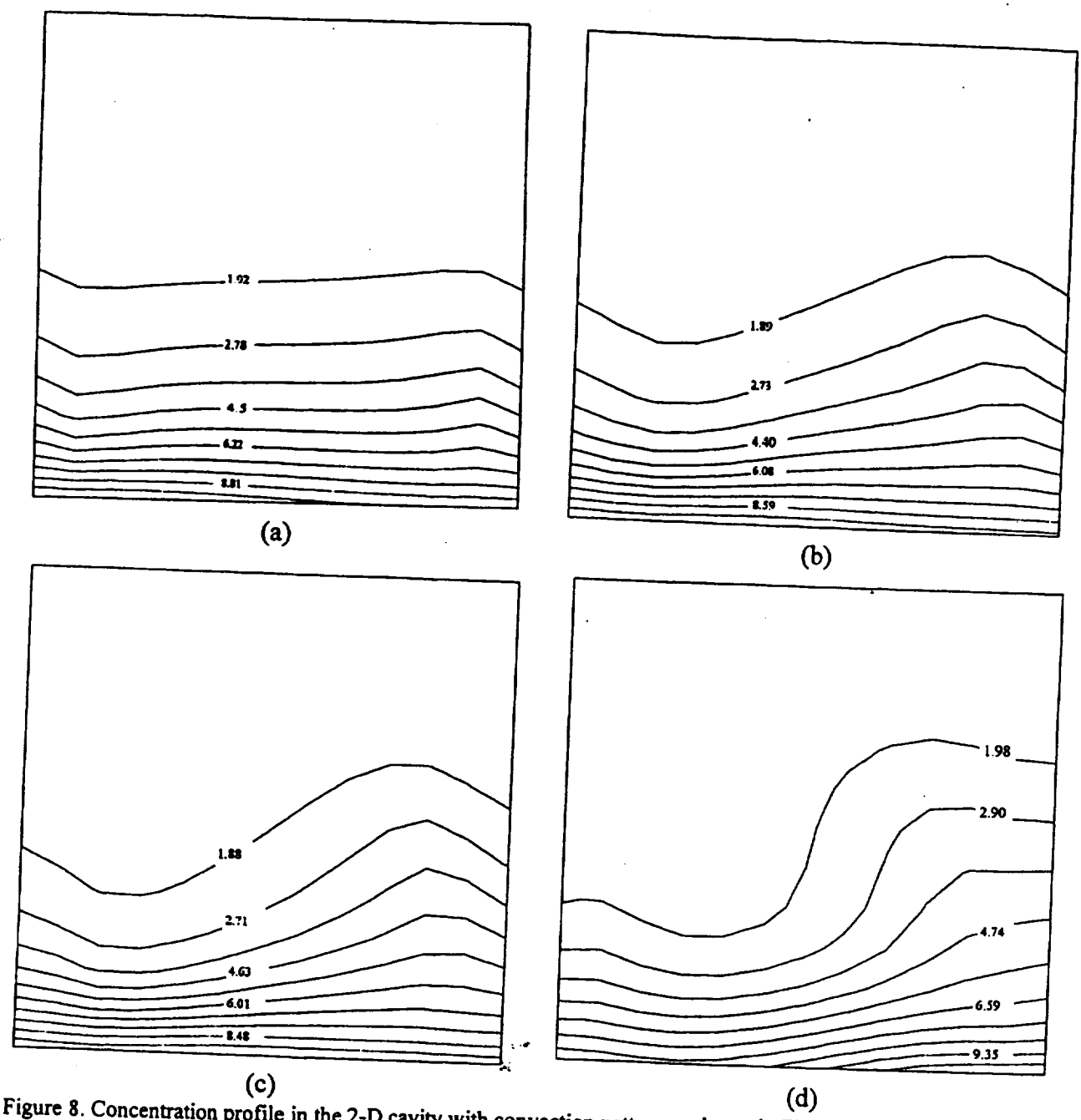

Figure 8. Concentration profile in the 2-D cavity with convection pattern as shown in Figure 4: (a) t = 0.5; (b) t = 1.75; (c) t = 2.5; (d) t = 10.25.

From the crystal growth point of view, the concentration distribution along the solidification front has an important implication to the impurity striation in the crystals grown. Figures 11 and 12 illustrate the effect of the applied magnetic field on the concentration distribution along the crystal-liquid interface (at z=0). With the absence of an external magnetic field (see Figure 11), the concentration profile oscillates with time along the interface and as large as 40% difference (|Cmax-Cmin/Cmean|) in concentration is observed at some instances, indicating the strong effect of convection in the liquid pool. With an applied magnetic field,

however, the oscillation is greatly reduced, and the concentration profile along the interface evolves over a much longer time period, suggesting that the convection effects are much reduced. Comparison of Figures 11 and 12 shows also that the oscillation in concentration distribution along the interface is reduced as a result of the application of a magnetic field.

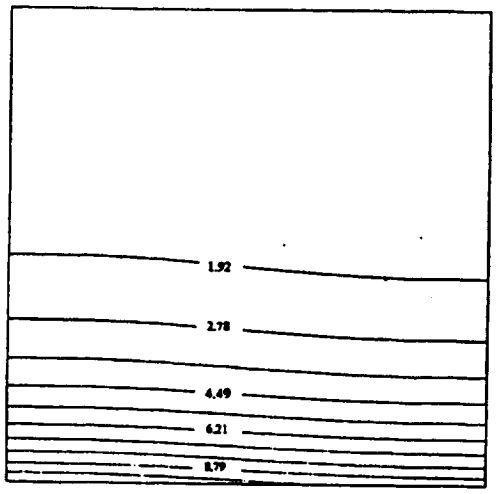

Figure 9. Concentration profile of multi-frequency g-jitter, with magnetic field Bx=0.22, Ha=100. The profile remains approximately the same for the time period as shown in Figure 6.

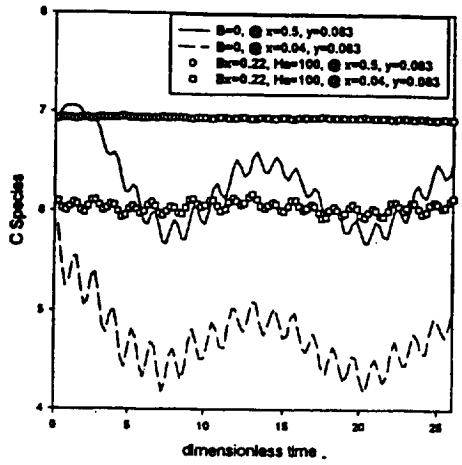

Figure 10. History of concentration change with time with and without magnetic field at certain points.

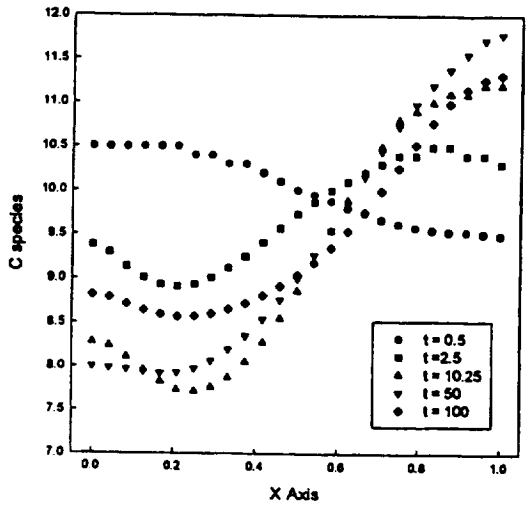

Figure 11. Concentration distribution along the interface at different times without imposed magnetic field.

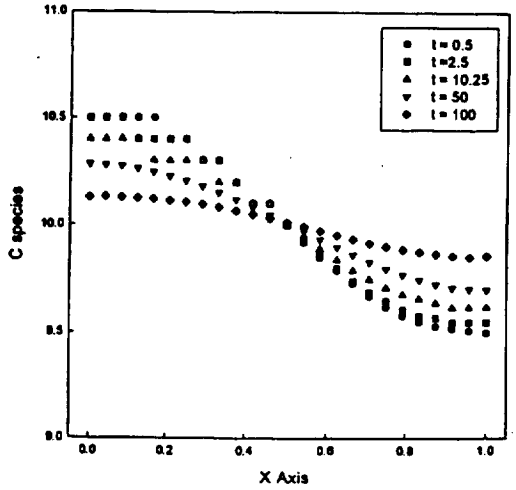

Figure 12. Concentration distribution along the interface at different times with a magnetic field Bx=0.22, Ha=100.

5. CONCULDING REMARKS

This paper has presented a finite element model for the transient fluid flow, heat transfer and solute transport in a 2-D cavity that is relevant to the Bridgmann-Stockbarger single crystal growth processes. The model predictions compared well with available analytical solutions. The numerical model was applied to study the fluid flow driven by g-jitter, heat transfer and solute redistribution. The numerical results obtained from the model showed that an applied magnetic field can have a significant effect on the convective flow and hence the solute redistribution in the system.

6. ACKNOWLEDGMENT

The authors gratefully acknowledge the support of this work by NASA (Grant #: NCC8-92).

7. REFERENCES

[1] HENRY C. DE GROH III AND EMILY S. NELSON. *On Residual Acceleration During Space Experiments*. ASME Winter Annual Meeting. Chicago, Nov 6-11, HTD-Vol 290, pp23-33. (1994)

[2] B. N. ANTAR and V. S. NUOTIO-ANTAR, *Fundamentals of low gravity fluid dynamics and heat transfer (CRC Press.* Boca Ration, FL (1993).

[3] STEFAN SCHNEIDER AND JOHANNES STRAUB *J. of Crystal .Growth* Vol 97 pp235-242, (1989)

[4] J.I.D. ALEXANDER, S. AMIROUDINE, J. QUAZZANI and F. ROSENBERGER, *J. Crystal Growth 113, 21-38.* (1991).

[5] J.I.D. ALEXANDER, J. QUAZZANI and F. ROSENBERGER, *J. Crystal Growth* 97, 285-302 (1989).

[6] E. S. NELSON, *An examination of anticipated g-jitter in space station and its effects on materials processes. NASA* TM 103775 (1991).

[7] J. CASADEMUNT, W. ZHANG, J. VENALS and R.F. SEKERKA, *AIAA J.* 31, 2027 (1993).

[8] W. ZHANG, J. CASADEMUNT, and J. VENALS, *J. Phys. Fluids,* A 5,3147 (1993).

[9] A.A. WHEELER, G.B. McFADDEN, B.T. MURRAY and S.R. CORIELL, *J. Phys. Fluids A* 3,2847 (1991).

[10] J.I.D. ALEXANDER, *Microgravity Sci. Tech.* 2,131 (1994).

[11] H. CHEN, M.Z. SAGHIR, D.H.H. QUON and S. CHEBAB, *J. Crystal Growth* 142,362 (1994).

[12] J. BAUMGARTL, M. GEWALD, R. RUPP, J. STIERLEN and G. MULLER, in *Proc. of VIth Euro. Symp. On Materials and Fluids Sciences in Microgravity,* p. 47. Oxford, UK (1990).

[13] R.W. SERIES and T.J. HURLE, *J. Crystal Growth* 113, 305 (1991).

[14] S. SCHNEIDER and J. STRAUB, *J. Crystal Growth* 97, 235-242 (1989).

[15] B. PAN and B. Q. Li *Effect of Magnetic fields on oscillation mixed convection.* Submitted

[16] S. CHANDRASEKHAR, *Hydrodynamic and Hydromagnetic Stability.* Dover, New York (1981).

[17] ZIENKIEWICZ, O. C. AND TAYLOR, R. L. *The Finite Element Method,* 4th Ed., McGraw-Hill, New York, NY. (1992)

[18] PAN, B. AND LI, B. Q. *Effects of magnetic field on oscillating mixed convection.* Int. J. Heat Mass Trans., submitted.